

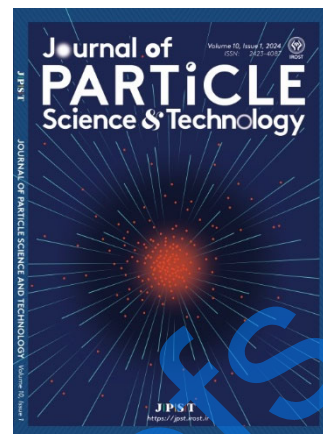
## Journal Pre-proofs

Sonochemical Synthesis of  $\gamma$ -Fe<sub>2</sub>O<sub>3</sub> Nanoparticles for Cancer Hyperthermia

Mahtab Farzaneh, Sayed Ali Hassanzadeh-Tabrizi, Nader Mokhtarian

DOI: <https://doi.org/10.22104/jpst.2025.7293.1267>

Manuscript number: JPST-2409-1262



To appear in: *Journal of Particle Science and Technology (JPST)*

Received Date: 20 December 2024

Received Date in revised form: 26 January 2025

Accepted Date: 28 February 2025

**Please cite this article as:** Farzaneh M., Hassanzadeh-Tabrizi S. A., Mokhtarian N., Sonochemical Synthesis of  $\gamma$ -Fe<sub>2</sub>O<sub>3</sub> Nanoparticles for Cancer Hyperthermia, *Journal of Particle Science and Technology* (2024), doi: <https://doi.org/10.22104/jpst.2025.7293.1267>

File of an article that has undergone enhancements after acceptance, such as the addition of a cover page and metadata, and formatting for readability, but it is not yet the definitive version of record. This version will undergo additional copyediting, typesetting and review before it is published in its final form, but we are providing this version to give early visibility of the article. Please note that, during the production process, errors may be discovered which could affect the content, and all legal disclaimers that apply to the journal pertain.

© 2024 The Author(s). Published by [IROST](#).

# Sonochemical synthesis of $\gamma$ -Fe<sub>2</sub>O<sub>3</sub> nanoparticles for cancer hyperthermia

Mahtab Farzaneh<sup>a</sup>, Sayed Ali Hassanzadeh-Tabrizi<sup>a,\*</sup>, Nader Mokhtarian<sup>b</sup>

<sup>a</sup> Advanced Materials Research Center, Department of Materials Engineering, Najafabad Branch, Islamic Azad University, Najafabad, Iran

<sup>b</sup> Department of Chemical Engineering, Shahreza Branch, Islamic Azad University, Shahreza, Iran

## Abstract

This study addresses the limitations of conventional cancer treatments, such as chemotherapy and radiotherapy, by focusing on the synthesis and characterization of superparamagnetic  $\gamma$ -Fe<sub>2</sub>O<sub>3</sub> nanoparticles (GMNP) using the sonochemical method for hyperthermia-based cancer therapy. While previous studies have explored the use of magnetic nanoparticles in cancer treatment, their efficiency and quality have remained suboptimal. In this study, we propose a sonochemical approach to enhance the quality and performance of GMNPs. The sonochemical method improved nanoparticle quality and efficiency. The GMNPs demonstrated a significant hyperthermic effect, with a temperature increase exceeding 43°C under an alternative magnetic field (that will be referred to as ACMF in abbreviations) (400 kHz), which can help induce apoptosis and necrosis in cancer cells. The nanoparticles were spherical in shape, with sizes ranging from 20 to 51 nm. Cytotoxicity assays (MTT assay) showed that the nanoparticles maintained high biocompatibility, with cell viability above 75% at all concentrations. These findings suggest that GMNPs synthesized via the sonochemical method offer improved efficacy compared to traditional methods, making them a promising candidate for hyperthermia-based cancer therapy.

**Keywords:**  $\gamma$ -Fe<sub>2</sub>O<sub>3</sub>, Nanoparticles, Hyperthermia, Cancer

## 1. Introduction

Cancer is the second leading cause of death worldwide and one of the greatest challenges to human health. Traditional treatment methods like chemotherapy are rapidly being replaced by innovative and targeted therapies. One such method is hyperthermia therapy, which involves using heat to increase the temperature of cancerous tumors to destroy them. This approach can be effective

either as a complement to or a replacement for conventional treatments, particularly for treating deep and resistant tumors. This method offers precise targeting of tumors, resulting in fewer side effects and preventing damage to healthy tissues. Additionally, it can serve as a complementary approach to other treatments such as chemotherapy and radiotherapy, enhancing their effectiveness. Due to its ability to penetrate deep into the body, hyperthermia is particularly useful for treating inaccessible deep tumors. Other advantages include the precise control of temperature and its customization for the destruction of cancer cells, leading to reduced treatment time [1,2].

In recent years, the use of magnetic nanoparticles has gained attention as one of the best tools for creating magnetic hyperthermia. In this method, magnetic nanoparticles are exposed to an alternating magnetic field, converting the field's energy into heat and raising the tumor's temperature. Unlike other hyperthermia methods (such as using ultrasound waves, microwave waves, etc.), which face challenges like low targeting precision and limited penetration into deep tumors, magnetic hyperthermia using magnetic nanoparticles resolves these issues and can accurately target deep-seated tumors [3-5].

In recent decades, the unique properties of magnetic iron oxide nanoparticles ( $\text{Fe}_2\text{O}_3$  and  $\text{Fe}_3\text{O}_4$ ) have expanded their application in clinical settings, particularly in cancer treatment. This is primarily due to their excellent intrinsic magnetic properties, nanoscale size, and ability to generate heat when exposed to an alternating magnetic field (AMF) [6,7]. Iron oxide ( $\text{Fe}_2\text{O}_3$ ) exists in various forms, such as maghemite ( $\gamma\text{-Fe}_2\text{O}_3$ ), hematite ( $\alpha\text{-Fe}_2\text{O}_3$ ),  $\beta\text{-Fe}_2\text{O}_3$ ,  $\delta\text{-Fe}_2\text{O}_3$ ,  $\eta\text{-Fe}_2\text{O}_3$ ,  $\varepsilon\text{-Fe}_2\text{O}_3$ , and oxide hydroxides like goethite ( $\alpha\text{-FeOOH}$ ) and lepidocrocite ( $\gamma\text{-FeOOH}$ ) [8]. Among these, maghemite nanoparticles ( $\gamma\text{-Fe}_2\text{O}_3$ ) hold significant importance in cancer treatment [9]. Due to their outstanding magnetic properties, high thermal stability, and resistance to oxidation, these nanoparticles are considered suitable for hyperthermia treatments. Compared to other iron nanoparticles like  $\text{Fe}_3\text{O}_4$ ,  $\gamma\text{-Fe}_2\text{O}_3$  nanoparticles exhibit higher magnetic saturation and resistance to phase changes at elevated temperatures, which is critical for hyperthermia treatments. Additionally, these nanoparticles can

generate the necessary heat to destroy cancer cells at high temperatures without losing efficiency [9-11].

Several methods have been employed to synthesize magnetic nanoparticles for hyperthermia, including chemical precipitation, solvothermal synthesis, and sol-gel processes [12]. However, these methods often face challenges in terms of control over nanoparticle size, morphology, and the uniformity of the magnetic properties. Given the high importance of magnetic nanoparticles in magnetic hyperthermia and their potential in cancer treatment, this study focuses on the production and characterization of  $\gamma\text{-Fe}_2\text{O}_3$  nanoparticles and their response to alternating magnetic fields for hyperthermia applications. The main objective of this research is to develop and improve synthesis methods for magnetic nanoparticles using a sonochemical approach. This method employs ultrasonic waves to enhance reaction rates, enabling the synthesis of higher-quality, more efficient nanoparticles [13]. This method uses ultrasonic radiation to increase the reaction rate and reduce synthesis time. Additionally, the creation of "acoustic cavitation" helps in better control of the size and uniform distribution of nanoparticles. Sonochemistry allows reactions to occur at low temperatures, which helps reduce energy consumption and improves the properties of temperature-sensitive nanoparticles. Moreover, this method does not require additional catalysts or stabilizers, which reduces costs and increases the purity of the final product. Furthermore, by precisely controlling the synthesis processes, the magnetic properties of the nanoparticles can be enhanced. Finally, sonochemistry is easily scalable and can be implemented in larger scales [14,15].

This study specifically focuses on the synthesis and characterization of  $\gamma\text{-Fe}_2\text{O}_3$  nanoparticles using the sonochemical method for hyperthermia-based cancer therapy. The main objective is to develop a more efficient and controlled synthesis approach for magnetic nanoparticles and to investigate their potential in cancer treatment. We aim to address key challenges such as ensuring nanoparticle stability in biological environments, controlling temperature within targeted tissues, and improving the therapeutic efficacy of magnetic hyperthermia.

## 2. Materials and methods

### 2.1. General

The sonochemical method used in this study for the synthesis of  $\gamma$ -Fe<sub>2</sub>O<sub>3</sub> nanoparticles was carried out using an ultrasonic device with a frequency of 30 kHz and an ultrasonic power of 250 W and equipped with a titanium probe. The ultrasonic process was carried out at room temperature. All chemicals used in the synthesis were of high purity and were purchased from reputable suppliers.

### 2.2. Materials

Iron nitrate nonahydrate (Fe(NO<sub>3</sub>)<sub>3</sub>·9H<sub>2</sub>O) with 98% purity from MERCK Germany, hydrazine monohydrate solution with 70% purity from Jiangsu Sopo China, and 96% ethanol from CMG Iran were used for the preparation of nanoparticles.

### 2.3. Preparation of nanoparticles

Contrary to other studies such as Yoon-Joo Lee et al., which used traditional chemical techniques to create  $\gamma$ -Fe<sub>2</sub>O<sub>3</sub> nanoparticles, this study uses a sonochemical method[16]. Traditional chemical techniques have problems such as high cost of raw materials, high volume of shrinkage and cracking during the drying process, lack of proper control over the size, shape, and morphology of the nanoparticles, etc. Meanwhile, the sonochemical technique offers a more regular and reproducible synthesis process by greatly increasing the particle size distribution and synthesis efficiency[17,18]. According to the findings by Maiti et al., To synthesize  $\gamma$ -Fe<sub>2</sub>O<sub>3</sub> nanoparticles, 40.4 grams of iron(III) nitrate nonahydrate (Fe(NO<sub>3</sub>)<sub>3</sub>·9H<sub>2</sub>O) were dissolved in 100 milliliters of deionized water. The solution was made at room temperature (25°C). The solution's initial pH was measured with a pH meter and found to be 1.56. Hydrazine monohydrate was then added dropwise to the solution, and after 45 minutes of stirring, when the pH reached 3.30, stirring was continued for an additional 15

minutes while the solution was ultrasonically treated (at 250 W and 30 kHz). This procedure increased the pH to 3.76. Hydrazine monohydrate was added again, and the solution was sonicated for another 15 minutes, during which time the color of the solution changed to dark brown and the pH rose to 5.12. Another dropwise addition of hydrazine monohydrate was added, and sonication was repeated for 2 hours, raising the pH to 7.12. To prevent the production of the Gamma phase of  $\text{Fe}_2\text{O}_3$ , avoid adding hydrazine monohydrate rapidly and in large quantities. The precipitate was washed with deionized water, followed by ethanol, then centrifuged at 10,500 rpm for 10 minutes. This procedure entailed washing the nanoparticles four times with deionized water and ethanol. Initially, the nanoparticles were washed with deionized water, followed by ethanol, and then washed two more times with deionized water to completely remove the ethanol from the nanoparticles. The centrifuged precipitate was dried in a hot air oven at 70°C for 72 hours. Finally, the dried product was ground into a fine powder using a mortar and pestle to obtain  $\gamma\text{-Fe}_2\text{O}_3$  nanoparticles [8].

#### 2.4. Characterizations

FTIR spectra of the magnetic nanoparticles (GMNPs) were recorded using a Jasco 6300 spectrophotometer (Japan). All samples were mixed with pure potassium bromide (KBr) powder, ground into fine powders, and pressed mechanically into semi-transparent disks. A pure KBr disk was used as the background. The FTIR spectra were recorded from 500  $\text{cm}^{-1}$  to 4000  $\text{cm}^{-1}$  with a resolution of 4  $\text{cm}^{-1}$ . The morphological features and particle size of GMNPs were evaluated using a CM120 transmission electron microscope (TEM, Netherlands). The microstructures and shapes of GMNPs were examined using a MIRA TESCAN field emission scanning electron microscope (FESEM) equipped with an EDS module. The crystalline structures of GMNPs were analyzed using a D8 ADVANCE X-ray diffraction (XRD) device from Bruker, Germany. The analysis was conducted over a range of  $2\theta$  (20–80°) using a copper monochromatic radiation source (wavelength 1.5406 Å) with a step size of 2° per minute. Additionally, to measure the magnetization curves and

magnetic properties of GMNPs, a vibrating sample magnetometer (VSM) model MDKB from Iran, with an applied field of  $\pm 20$  kOe at room temperature, was used.

### 2.5. Hyperthermia assay

To evaluate the hyperthermia properties of the nanoparticles, a hyperthermia device manufactured by Magnatis Danesh Pouya Kashan, Iran, was used. This test was performed under a magnetic field intensity of 400 Oersted, with a frequency of approximately 400 kHz for 5 minutes at room temperature. Initially, various nanoparticle concentrations were tested to determine the optimal concentration for effective hyperthermia treatment. Ultimately, a concentration of 120 mg/mL was selected as the optimal concentration. The heat induction of nanoparticles, represented by the specific loss power (SLP) factor, was calculated using Equation 1[19]. The temperature increase of the nanoparticles follows the Néel and Brownian laws. At the start of this test, the environment is adiabatic, and heat does not escape. The output of the test is the temperature change of the sample over time. It is worth noting that this test requires sample preparation, where the nanoparticles are dispersed in their base solution for 8 minutes.

$$SLP = \frac{C * 1000 * \Delta T}{Concentration * Time (S)} \quad (1)\#$$

Where,  $\Delta T$  is the temperature change before and after applying the magnetic field ( $^{\circ}C$ ),  $C$  is the specific heat capacity of the water.

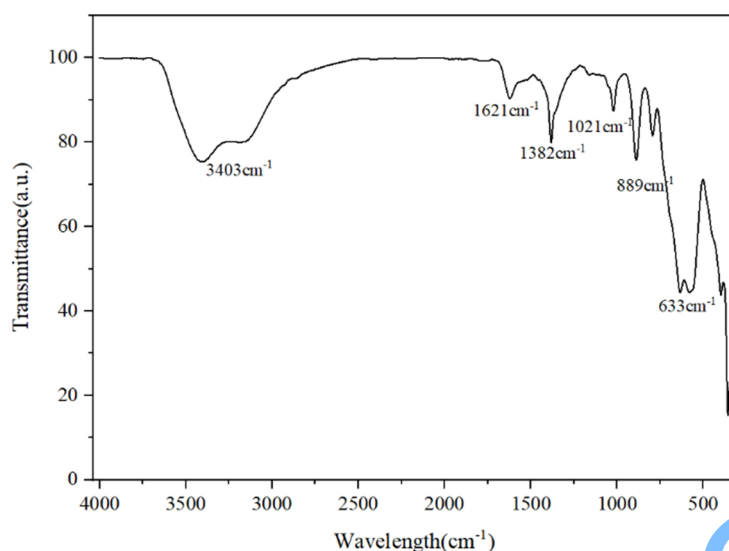
### 2.6. Cell viability assays

The MTT assay was used to assess the biocompatibility of the nanoparticles. OVCAR3 cell lines with a density of  $6 \times 10^4$  cells in DMEM supplemented with 10% FBS were seeded in a 96-well plate and incubated for 12 hours. The cells were then treated with GMNPs for 24, 48, and 72 hours. After

discarding the medium, 200 microliters of culture medium with 10 mg/mL MTT was added to each well and incubated at 37°C for 2 hours. This test was conducted using an extraction method.

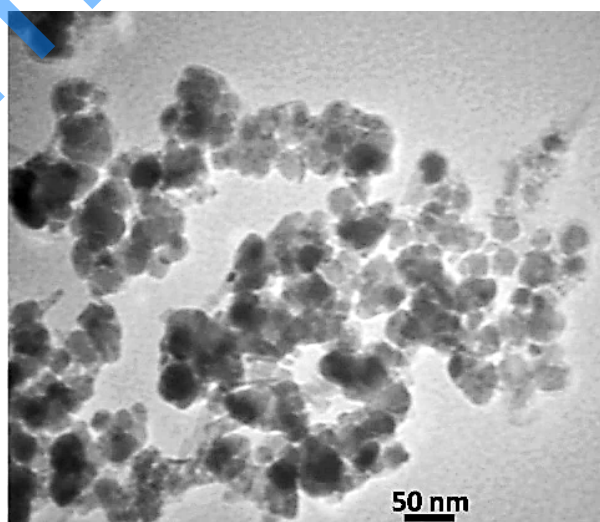
### 3. Results and discussion

Figure 1 shows the FTIR spectroscopy results of  $\gamma$ -Fe<sub>2</sub>O<sub>3</sub> nanoparticles (GMNPs). In order to confirm the accurate production of synthesized  $\gamma$ -Fe<sub>2</sub>O<sub>3</sub> nanoparticles, the FTIR spectrum of a standard Fe<sub>2</sub>O<sub>3</sub> sample was also analyzed and compared with the synthesized sample. The peaks at 1621 cm<sup>-1</sup>, 3403 cm<sup>-1</sup>, 633 cm<sup>-1</sup>, and others in the synthesized sample closely match those observed in the standard Fe<sub>2</sub>O<sub>3</sub> spectrum, confirming the successful synthesis of high-purity  $\gamma$ -Fe<sub>2</sub>O<sub>3</sub> nanoparticles. However, slight differences in peak intensities and positions could indicate the presence of residual species or slight variations in the synthesis process, which were further discussed [20, 21]. The peak at 1621 cm<sup>-1</sup> corresponds to the bending vibrations ( $\delta$ ) of water molecules adsorbed on the surface of pure GMNPs. The peak at 3403 cm<sup>-1</sup> is attributed to the stretching vibrations ( $\nu$ ) of O-H bonds [22]. Additionally, the peak at 633 cm<sup>-1</sup> corresponds to the stretching vibration mode of Fe-O bonds in the FTIR spectrum [23,24]. A very small peak at 1382 cm<sup>-1</sup> and 1021 cm<sup>-1</sup> is associated with residual nitrate ions adsorbed on the sample during preparation. Moreover, a fine peak at 889 cm<sup>-1</sup> indicates a small amount of Fe-OOH in the prepared  $\gamma$ -Fe<sub>2</sub>O<sub>3</sub> sample [25-28]. The results show that all major peaks related to GMNPs are visible, confirming that the nanoparticles have high purity and acceptable quality. The results obtained are consistent with those of Sohrabijam et al., and Lotfar Rahman *et al* [29,30].



**Figure 1.** FTIR spectrum of  $\gamma$ -Fe<sub>2</sub>O<sub>3</sub> (GMNPs).

Figure 2 displays TEM image of GMNPs. As shown, the GMNPs exhibit spherical shapes with particle sizes ranging from approximately 20 to 51 nanometers. According to research findings, spherical particles are more biocompatible with human cells and pose a lower risk of carcinogenicity, immune system activation, and cytotoxicity compared to rod-shaped or other morphologies [31]. The aggregation of particles is observed due to the very small size and high magnetic properties of the nanoparticles. This phenomenon arises because nanoparticles, having high surface energy, tend to aggregate to reduce their surface energy.



**Figure 2.** TEM image of GMNPs

This study demonstrates a well-defined size range of 20 to 51 nm, which is ideal for hyperthermia applications due to improved biocompatibility and controlled clearance from the body, as opposed to studies such as Debabrata Maiti *et al.*, where the particle size distribution of the synthesized nanoparticles was not precisely controlled. Furthermore, past studies may have failed to properly describe the appropriate size of nanoparticles for hyperthermia treatment. The results show that our nanoparticle size is ideal for hyperthermia applications, as nanoparticles smaller than 20 nm are easily eliminated by the kidneys, whereas nanoparticles larger than 100 nm can produce negative effects [13,32].

As illustrated in Figure 3, XRD analysis was conducted on the GMNPs to study the crystal structure of the products. The main peaks of  $\gamma$ -Fe<sub>2</sub>O<sub>3</sub> were observed at angles of 26.8°, 30.25°, 35.75°, 43.37°, 53.8°, 57.45°, and 63.09°. These angles correspond to the crystal planes (210), (220), (311), (400), (422), (440), and (511), confirming the successful formation of  $\gamma$ -Fe<sub>2</sub>O<sub>3</sub> consistent with reference card no. (0064-591-96) [33]. The results indicate no other phases formed, ensuring high purity of the nanoparticles. The crystal size was calculated using the Scherrer equation (Equation 2), resulting in approximately 15.8 nm.

$$D = \frac{K \lambda}{\beta \cos \theta} \quad (2)$$

Where D is crystallite size (nm), K is the Scherrer constant,  $\lambda$  is the X-ray wavelength (nm),  $\theta$  is the diffraction angle, and  $\beta$  is the peak width at half maximum intensity (FWHM). Reports suggest that magnetic properties of ferrites, such as coercivity, strongly depend on the average crystallite size. The critical size of the crystallites may represent the boundary for transitioning from multidomain to single-domain structures [34, 35] The calculated crystallite size was smaller than the particle size obtained from TEM images. This discrepancy between XRD and TEM results could be due to the

Scherrer equation not accounting for peak broadening caused by lattice strains [36]. The findings are comparable to those of Lutfur Rahman et al. and Sohrabijam et al [29, 30].

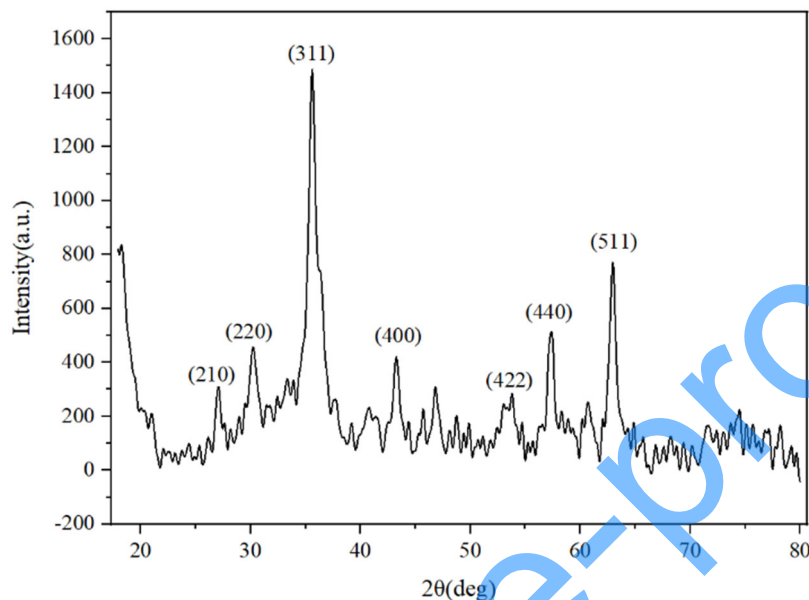
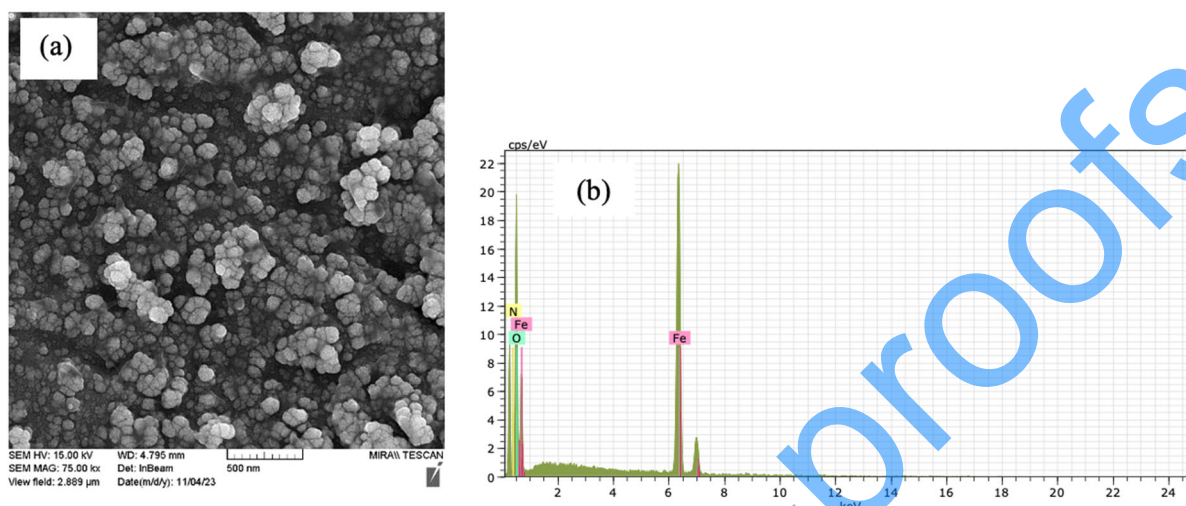


**Figure 3.** XRD patterns of GMNPs.

The size, shape, and morphology of the nanoparticles were examined using FESEM, as shown in Figure 4. The FESEM images reveal small, spherical particles with homogeneous sizes and a morphology resembling flowers [23, 37, 38]. Some dense nanoparticles, similar to TEM images, result from their high surface energy and superparamagnetic properties. Additionally, the nanoparticles generally have smooth or slightly uneven surfaces. Magnetic spherical nanoparticles offer significant advantages over rod-shaped or other morphologies in terms of biocompatibility and toxicity. This may be due to several factors. Firstly, spherical nanoparticles have a smaller specific surface area compared to rod-shaped particles. This can reduce their interaction with reactive regions, thereby decreasing toxicity and adverse interactions with biological systems. Additionally, spherical nanoparticles are more easily and uniformly absorbed by cells, which can improve their distribution

throughout the body. This uniformity can lead to more predictable and controlled biological responses, reducing the likelihood of localized toxicity [37, 39].



El	AN	unn. [wt.%]	C norm. [wt.%]	C Atom. [at.%]	C Error (1 Sigma) [wt.%]
Fe	26	48.01	56.97	27.50	1.34
O	8	36.26	43.03	72.50	5.65
N	7	0.00	0.00	0.00	0.00

**Figure 4.** (a) FESEM image and (b) EDS analysis of GMNPs.

Moreover, spherical nanoparticles can move more efficiently through the bloodstream, reducing the risk of their aggregation and allowing them to be more effectively cleared by the reticuloendothelial system. Consequently, the risk of their accumulation in organs is diminished. Furthermore, the shape of nanoparticles influences how they are recognized by the immune system. In general, nanoparticle size is a critical parameter for circulation lifetime. It has been reported that the optimal size of nanoparticles is typically between 20 to 200 nanometers, as smaller particles are quickly removed from the bloodstream by the kidneys, and larger particles are rapidly absorbed by macrophages, resulting in a shorter circulation lifespan [38]. Additionally, the EDS spectra of

GMNPs revealed the elemental composition of the sample. It is observed that iron, nitrogen, and oxygen are the main elements in the structure of the GMNPs. These results further confirm the presence and purity of  $\gamma$ -Fe<sub>2</sub>O<sub>3</sub> nanoparticles and showed good agreement with the XRD results and reported studies. The short peak observed around 7 keV corresponds to gold, which is due to the sample preparation process for FESEM.

Magnetic properties of GMNPs were examined at room temperature using VSM, as illustrated in Figure 5 a. The saturation magnetization of GMNPs was approximately 41 emu/g, demonstrating superparamagnetic behavior. Upon the application of an external magnetic field, the material becomes magnetized, but the magnetization disappears upon removing the field. This behavior results from the small particle size, which allows for random magnetic orientation in response to external fields [40]. Also, the strong response of GMNPs to the magnet can be seen in Figure 5 b. The results of the VSM experiment and the demonstration of the superparamagnetic property of GMNP are consistent with the results of Lutfur Rahman *et al* [29].

Figure 6 and Table 1 show the results of hyperthermia testing under in vitro and laboratory conditions. To achieve the optimal concentration of GMNPs for hyperthermia applications, three concentrations (5, 10, and 20 mg/mL nanoparticles) were tested for 5 minutes in pure water under hyperthermia conditions. The results indicate that higher GMNP concentrations cause greater temperature increases within 5 minutes. Specifically, the 20 mg/mL nanoparticle concentration yielded the highest temperature rise during the 5 minute duration. Thus, it can be concluded that these nanoparticles are a suitable and efficient choice for hyperthermia, and even at a concentration of 5 mg/mL, they can raise tumor temperatures to over 43 °C. It is evident that higher concentrations, such as 10 or 20 mg/mL, result in faster and greater temperature increases. The 20 mg/mL concentration is selected as the optimal concentration for temperature rise and hyperthermia effect.

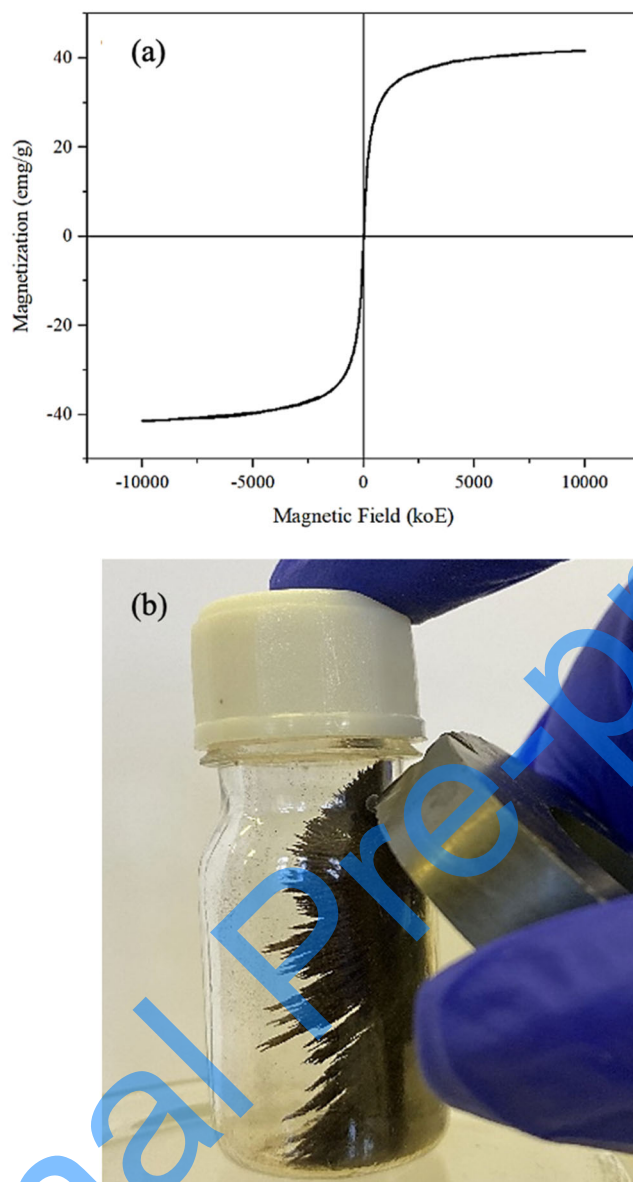


**Figure 5.** (a) Magnetic properties of GMNPs and (b) effect of magnet on the nanopowders.

As the GMNP concentration increases, the number of nanoparticles in a given volume also rises. Each nanoparticle, when exposed to a variable magnetic field, generates more magnetic energy, which is released as heat in the system. In fact, magnetic nanoparticles dynamically alter their magnetic orientations under the influence of an external magnetic field. These changes in magnetic orientation produce energy, which is released as heat. Consequently, as nanoparticle concentration increases, a greater temperature rise is observed in the material[41,42]. At higher concentrations,

nanoparticles are closer to one another, which may lead to magnetic interactions between the nanoparticles. These interactions can make the nanoparticles absorb and convert energy into heat more effectively. Moreover, at higher concentrations, the likelihood of magnetic interactions between nanoparticles increases, enhancing the thermal effect [43]. On the other hand, at lower concentrations, heat dispersion and energy transfer may not occur efficiently. However, at higher concentrations, the larger number of nanoparticles ensures more effective heat transfer within the system, leading to an overall temperature increase in the material[44, 45] . The SLP value was calculated to be 9.1 W/g. Our results are consistent with those of Lemine et al., who also used maghemite nanoparticles together with titanium oxide to produce a hyperthermia effect[46]. Another study by Fatima et al. produced high-performance Maghemite/poly(D,L-lactide-co-glycolide)/chitosan nanoparticles with an average size of 325nm. These nanocomposites displayed magnetic properties and functioned as T2 contrast agents in magnetic resonance imaging, as well as strong thermal capabilities for anticancer hyperthermia [47].

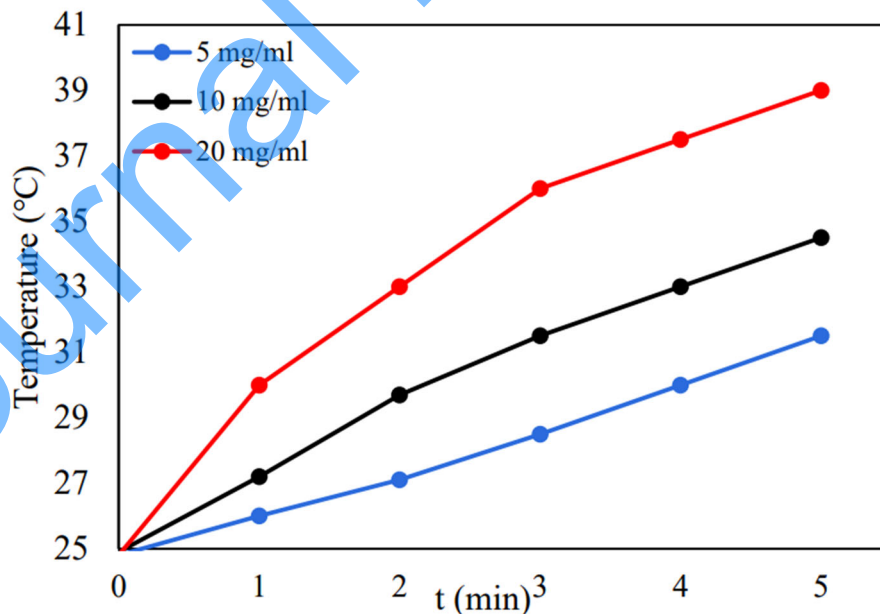


**Figure 6.** Hyperthermia test results for GMNPs.

**Table 1.** Temperature changes of the mixture under different nanoparticle concentrations

GMNPs Concentration (mg/ml)	T <sub>0</sub> (°C)	T <sub>1</sub> (°C)	T (°C)Δ
5#	25#	31.5#	6.5#
10#	25#	34.5#	9.5#
20#	25#	39#	14#

As mentioned, the cytotoxicity test was conducted on OVCAR3 cell lines<sup>1</sup> with a density of  $6 \times 10^4$  cells in DMEM containing 10% FBS in a 96-well plate. The GMNPs were dissolved in PBS (Phosphate Buffered Saline) before being added to the cell culture for MTT test. The main reagent for this test is tetrazolium, which is used in solution with PBS. This yellow solution is highly light-sensitive and, due to its net positive charge, is absorbed by cell membranes. It then enters the cell through endocytosis and reaches the mitochondria. This compound is converted by the enzyme succinate dehydrogenase, which is present in the mitochondria and active only in the respiratory chain of living cells, into purple water-insoluble formazan deposits. Essentially, out of many cells present, only living cells can convert the MTT solution into purple water-insoluble formazan precipitate. The optical density of the resulting solution can be measured using a spectrophotometer at 579 nm. The resulting value represents the absorbance of the purple formazan dye. To calculate the percentage of cell viability, the absorbance values of control samples (blank samples) and test samples are required. In the MTT assay, the blank consists of a cell-free medium plus an MTT solution and a solubilizing buffer. The blank represents the absorbance generated by the medium itself, which must be subtracted from the final values of the samples, standard curves, and positive and negative controls. Without accounting for the blank and subsequently subtracting its values from the experimental results, the MTT assay would not be accurate [48]. As shown in Figure 7, three different concentrations of GMNPs (5, 10, and 20 mg/mL) were examined. The MTT assay results showed that for all samples,

---

1- The OVCAR-3 cells are from a cell line derived from a malignant tumor of the ovary and they obtained from human ovarian cancer.

the percentage of cell viability was above 75% over the entire 72 hours. This result indicates that the nanoparticles at all concentrations are not cytotoxic. With increasing nanoparticle concentration, the percentage of cell viability slightly decreases. This reduction in viability may be due to the production of free radicals and oxidative stress caused by nanoparticles at higher concentrations. However, it is observed that even at the highest concentration (20 mg/mL), the viability percentage remains above 75%. Therefore, the produced samples are free from cytotoxic effects and can be easily injected for hyperthermia treatment. Sharifi et al.'s results demonstrate the non-cytotoxicity of maghemite nanoparticles at various doses, which is consistent with our findings. They contacted the nanoparticles with a breast cancer cell line(4T1), and the results showed that the nanoparticles did not cause any cytotoxicity and maintained cell viability at levels above 70%[49].

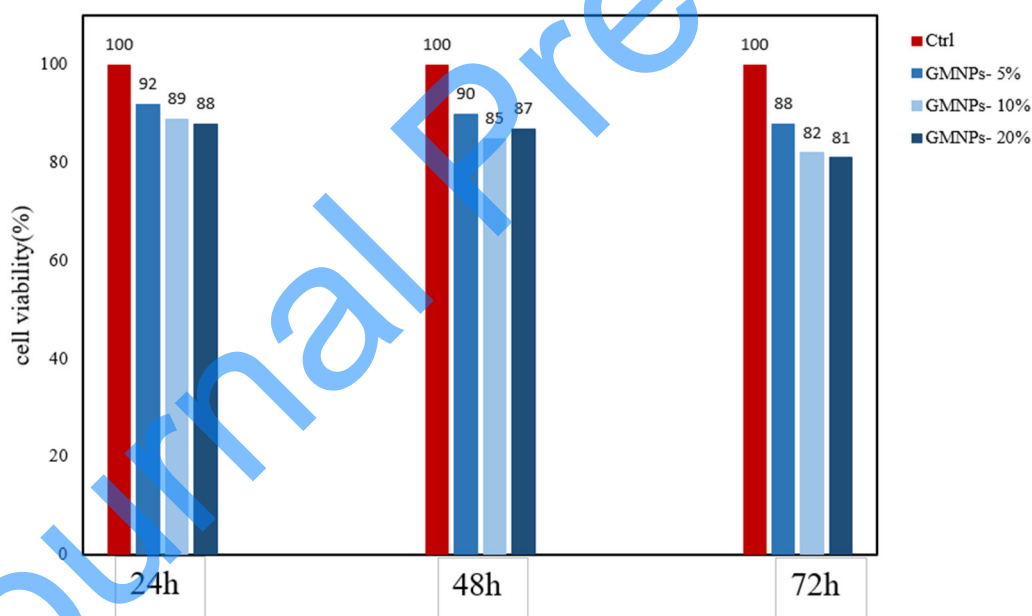


**Figure 7.** MTT assay results for GMNPs.

#### 4. Conclusion

In this study,  $\gamma\text{-Fe}_2\text{O}_3$  magnetic nanoparticles were successfully synthesized using the sonochemical method for potential tumor treatment using hyperthermia effect. The produced

nanoparticles exhibited superparamagnetic properties and were characterized by various techniques, including FTIR, XRD, VSM, TEM, and FE-SEM/EDS spectroscopy. TEM analysis confirmed nanoparticle dimensions in the range of 20–50 nm. Cytotoxicity testing on OVCAR3 cells found that the nanoparticles had no toxicity. Hyperthermia tests revealed that when exposed to an alternating magnetic field at 400 Oe and 400 kHz, the nanoparticles caused a temperature increase of around 14 °C within 5 minutes. These findings confirm the potential of  $\gamma$ -Fe<sub>2</sub>O<sub>3</sub> nanoparticles as a promising candidate for hyperthermia applications in cancer therapy.

However, several limitations must be recognized. First, the synthesis and characterization methods, although effective, were limited in terms of scalability and potential batch-to-batch variability, which could affect reproducibility in larger-scale manufacturing. Additionally, the in vitro studies were performed using only the OVCAR3 cell line, and future studies should explore the response of other cancer cell lines to assess the generalizability of these results. It is also necessary to investigate how apoptosis and cell death occur when applying a magnetic field to nanoparticles and causing hyperthermia on different cell lines. The hyperthermia experiments, while promising, were conducted under controlled conditions, and further testing in more complex environments is needed to evaluate the nanoparticles' behavior in vivo. As a future perspective, several avenues can be explored to enhance the clinical efficacy of these nanoparticles. In vivo studies are essential to evaluate the efficacy and safety of nanoparticles in animal models and provide more precise insight into their therapeutic potential. Optimization of the size and shape of nanoparticles may also enhance their hyperthermic performance. Finally, exploring combination therapies, such as using these nanoparticles in combination with chemotherapy, cell therapy, and immunotherapy, could provide more effective treatment strategies for cancer. Overall, the  $\gamma$ -Fe<sub>2</sub>O<sub>3</sub> nanoparticles synthesized in this study demonstrate excellent potential for hyperthermia-based cancer therapy.

**References**

- [1] Baronzio, G., et al., *A brief overview of hyperthermia in cancer treatment*. J Integr Oncol, 2014. 3(115): p. 2.
- [2] Peiravi, M., et al., *Magnetic hyperthermia: Potentials and limitations*. Journal of the Indian Chemical Society, 2022. 99(1): p. 100269.
- [3] Sarani, M., et al., *In vitro cytotoxic study of synthesized Ag and Ce dual-doped  $\alpha$ -Fe<sub>2</sub>O<sub>3</sub> nanoparticles on NIH/3T3 and U87 cell lines*. Inorganic Chemistry Communications, 2024. 170: p. 113236.
- [4] Mehdigholami, S. and E. Koohestanian, *Fe<sub>3</sub>O<sub>4</sub>@ SiO<sub>2</sub>/AEPTMS/Fe (OTf)<sub>3</sub>: An efficient superparamagnetic nanocatalyst for the protecting of alcohols*. Journal of Particle Science and Technology, 2023. 9(1): p. 1-9.
- [5] Koohestanian, E. and S. Mehdigholami, *Synthesis of Hematite Nanoparticles by Ball Milling and the Study of the Magnetic Properties and its Microstructure*. Chemical Process Design, 2023. 2(2): p. 52-59.
- [6] Gupta, A.K. and M. Gupta, *Synthesis and surface engineering of iron oxide nanoparticles for biomedical applications*. biomaterials, 2005. 26(18): p. 3995-4021.
- [7] Mohassel, R., et al., *Pechini synthesis using propylene glycol and various acid as stabilizing agents and characterization of Gd<sub>2</sub>NiMnO<sub>6</sub> ceramic nanostructures with good photocatalytic properties for removal of organic dyes in water*. Journal of Materials Research and Technology, 2020. 9(2): p. 1720-1733.
- [8] Sakurai, S., et al., *First observation of phase transformation of all four Fe<sub>2</sub>O<sub>3</sub> phases ( $\gamma \rightarrow \varepsilon \rightarrow \beta \rightarrow \alpha$ -phase)*. Journal of the American Chemical Society, 2009. 131(51): p. 18299-18303.
- [9] Vangijzegem, T., D. Stanicki, and S. Laurent, *Magnetic iron oxide nanoparticles for drug delivery: applications and characteristics*. Expert opinion on drug delivery, 2019. 16(1): p. 69-78.

- [10] Hugounenq, P., et al., *Iron oxide monocrystalline nanoflowers for highly efficient magnetic hyperthermia*. The Journal of Physical Chemistry C, 2012. 116(29): p. 15702-15712.
- [11] Zinatloo-Ajabshir, S., et al., *A green route for the synthesis of sponge-like Pr<sub>6</sub>O<sub>11</sub> nanoparticles and their application for the development of chlorambucil sensor*. Measurement, 2024. 235: p. 114924.
- [12] Baladi, M., et al., *Green sol-gel synthesis of hydroxyapatite nanoparticles using lemon extract as capping agent and investigation of its anticancer activity against human cancer cell lines (T98, and SHSY5)*. Arabian Journal of Chemistry, 2023. 16(4): p. 104646.
- [13] Maiti, D., et al., *Phase evolution and growth of iron oxide nanoparticles: effect of hydrazine addition during sonication*. Crystal growth & design, 2013. 13(8): p. 3637-3644.
- [14] Joshi, N., et al., *Metal oxide nanoparticles: synthesis, properties, characterization, and applications*, in *Nanomaterials: advances and Applications*. 2023, Springer. p. 103-144.
- [15] Islam, M.H., et al., *Recent developments in the sonoelectrochemical synthesis of nanomaterials*. Ultrasonics sonochemistry, 2019. 59: p. 104711.
- [16] Lee, Y.-J., et al., *A simple chemical route for the synthesis of  $\gamma$ -Fe<sub>2</sub>O<sub>3</sub> nano-particles dispersed in organic solvents via an iron-hydroxy oleate precursor*. Journal of Industrial and Engineering Chemistry, 2008. 14(1): p. 38-44.
- [17] Nomngongo, P.N., *Nanoadsorbents: synthesis, characterization, and industrial applications*, in *Adsorption through Advanced Nanoscale Materials*. 2023, Elsevier. p. 23-45.
- [18] Carter, C.B. and M.G. Norton, *Sols, gels, and organic chemistry*. Ceramic Materials: Science and Engineering, 2007: p. 400-411.
- [19] Halgamuge, M.N. and T. Song, *Optimizing heating efficiency of hyperthermia: Specific loss power of magnetic sphere composed of superparamagnetic nanoparticles*. Progress In Electromagnetics Research B, 2020. 87: p. 1-17.

- [20] Noor Azreen, A.R., et al., *Synthesis and Characterization of Fe<sub>2</sub>O<sub>3</sub> Prepared Via Sol-Gel Method*. Advanced Materials Research, 2012. 545: p. 410-413.
- [21] Lemine, O., *Microstructural characterisation of  $\alpha$ -Fe<sub>2</sub>O<sub>3</sub> nanoparticles using, XRD line profiles analysis, FE-SEM and FT-IR*. Superlattices and Microstructures, 2009. 45(6): p. 576-582.
- [22] Hassanzadeh-Tabrizi, S. and E. Taheri-Nassaj, *Polyacrylamide gel synthesis and sintering of Mg<sub>2</sub>SiO<sub>4</sub>: Eu<sup>3+</sup> nanopowder*. Ceramics International, 2013. 39(6): p. 6313-6317.
- [23] Espinoza, M.J.C., et al., *In vitro studies of Pluronic F127 coated magnetic silica nanocarriers for drug delivery system targeting liver cancer*. European Polymer Journal, 2021. 153: p. 110504.
- [24] Hassanzadeh-Tabrizi, S., *Synthesis of NiFe<sub>2</sub>O<sub>4</sub>/Ag nanoparticles immobilized on mesoporous g-C<sub>3</sub>N<sub>4</sub> sheets and application for degradation of antibiotics*. Journal of Photochemistry and Photobiology A: Chemistry, 2021. 418: p. 113398.
- [25] Qian, Z., et al., *In situ injectable thermoresponsive nanocomposite hydrogel based on hydroxypropyl chitosan for precise synergistic calcium-overload, photodynamic and photothermal tumor therapy*. Carbohydrate Polymers, 2024. 324: p. 121487.
- [26] Golmohammad, M., F. Golestanifard, and A. Mirhabibi, *Synthesis and characterization of maghemite as an anode for lithium-ion batteries*. Int. J. Electrochem. Sci, 2016. 11: p. 6432-6442.
- [27] Nazari, M., et al., *Synthesis and characterization of maghemite nanopowders by chemical precipitation method*. Journal of Nanostructure in Chemistry, 2014. 4: p. 1-5.
- [28] Wattanathana, W., et al., *Crystallographic and spectroscopic investigations on oxidative coordination in the heteroleptic mononuclear complex of cerium and benzoxazine dimer*. Molecules, 2021. 26(17): p. 5410.
- [29] Rahman, L., et al., *A study on the preparation and characterization of maghemite ( $\gamma$ -Fe<sub>2</sub>O<sub>3</sub>) particles from iron-containing waste materials*. Journal of Asian Ceramic Societies, 2020. 8(4): p. 1083-1094.

- [30] Sohrabijam, Z., et al., *Preparation and characterization of superparamagnetic chitosan coated maghemite ( $\gamma$ -Fe<sub>2</sub>O<sub>3</sub>) for gene delivery*. *Procedia Materials Science*, 2015. 11: p. 282-286.
- [31] Lee, J.H., et al., *Rod-shaped iron oxide nanoparticles are more toxic than sphere-shaped nanoparticles to murine macrophage cells*. *Environmental Toxicology and Chemistry*, 2014. 33(12): p. 2759-2766.
- [32] Singh, R. and S.V. Torti, *Carbon nanotubes in hyperthermia therapy*. *Advanced drug delivery reviews*, 2013. 65(15): p. 2045-2060.
- [33] Kafle, B.P., *Introduction to nanomaterials and application of UV-Visible spectroscopy for their characterization*. *Chemical analysis and material characterization by spectrophotometry*, 2020. 6: p. 147-198.
- [34] Upadhyay, S., K. Parekh, and B. Pandey, *Influence of crystallite size on the magnetic properties of Fe<sub>3</sub>O<sub>4</sub> nanoparticles*. *Journal of Alloys and Compounds*, 2016. 678: p. 478-485.
- [35] Li, Q., et al., *Correlation between particle size/domain structure and magnetic properties of highly crystalline Fe<sub>3</sub>O<sub>4</sub> nanoparticles*. *Scientific reports*, 2017. 7(1): p. 9894.
- [36] Hu, C., et al., *Direct synthesis and structure characterization of ultrafine CeO<sub>2</sub> nanoparticles*. *Nanotechnology*, 2006. 17(24): p. 5983.
- [37] Ma, N., et al., *Influence of nanoparticle shape, size, and surface functionalization on cellular uptake*. *Journal of nanoscience and nanotechnology*, 2013. 13(10): p. 6485-6498.
- [38] Cooley, M., et al., *Influence of particle size and shape on their margination and wall-adhesion: implications in drug delivery vehicle design across nano-to-micro scale*. *Nanoscale*, 2018. 10(32): p. 15350-15364.
- [39] Love, S.A., et al., *Assessing nanoparticle toxicity*. *Annual review of analytical chemistry*, 2012. 5(1): p. 181-205.

- [40] Vijayasri, G., R.C. Bhaskar, and J. Rajesh, *An essential advancement of magnetic nanoparticles*, in *Fundamentals and Industrial Applications of Magnetic Nanoparticles*. 2022, Elsevier. p. 41-63.
- [41] Pucci, C., et al., *Superparamagnetic iron oxide nanoparticles for magnetic hyperthermia: Recent advancements, molecular effects, and future directions in the omics era*. *Biomaterials Science*, 2022. 10(9): p. 2103-2121.
- [42] Abenojar, E.C., et al., *Structural effects on the magnetic hyperthermia properties of iron oxide nanoparticles*. *Progress in Natural Science: Materials International*, 2016. 26(5): p. 440-448.
- [43] Obaidat, I.M., B. Issa, and Y. Haik, *Magnetic properties of magnetic nanoparticles for efficient hyperthermia*. *Nanomaterials*, 2015. 5(1): p. 63-89.
- [44] Dennis, C.L. and R. Ivkov, *Physics of heat generation using magnetic nanoparticles for hyperthermia*. *International Journal of Hyperthermia*, 2013. 29(8): p. 715-729.
- [45] Chakraborty, A.R., et al., *Influence of annealing temperature on Fe<sub>2</sub>O<sub>3</sub> nanoparticles: Synthesis optimization and structural, optical, morphological, and magnetic properties characterization for advanced technological applications*. *Heliyon*, 2024. 10(21).
- [46] Lemine, O., et al., *Maghemite ( $\gamma$ -Fe<sub>2</sub>O<sub>3</sub>) and  $\gamma$ -Fe<sub>2</sub>O<sub>3</sub>-TiO<sub>2</sub> nanoparticles for magnetic hyperthermia applications: Synthesis, characterization and heating efficiency*. *Materials*, 2021. 14(19): p. 5691.
- [47] Fernández-Álvarez, F., et al., *Engineering of stealth (maghemite/PLGA)/chitosan (core/shell)/shell nanocomposites with potential applications for combined MRI and hyperthermia against cancer*. *Journal of Materials Chemistry B*, 2021. 9(24): p. 4963-4980.
- [48] Supino, R., *MTT assays*. *In vitro toxicity testing protocols*, 1995: p. 137-149.
- [49] Sharifi, M., et al., *Fabrication and evaluation of anti-cancer efficacy of lactoferrin-coated maghemite and magnetite nanoparticles*. *Journal of Biomolecular Structure and Dynamics*, 2020. 38(10): p. 2945-2954.